On the effectiveness of a quasistatic bubble-scale simulation in predicting the constriction flow of a two-dimensional foam

S. A. Jones[a] and S. J. Cox[b]

Institute of Mathematics and Physics, Aberystwyth University, Aberystwyth, Ceredigion SY23 3BZ, United Kingdom

(Received 9 September 2011; final revision received 29 January 2012; published 20 March 2012)

Synopsis

A comprehensive set of experiments on a two-dimensional constriction flow of a foam are described. Image analysis of the flow is used to ascertain bubble shape and flow dynamics. The bubble velocity, elongation (texture), stress, and deformation rate for a reference case are used to validate a quasistatic simulation. Changes to the constriction geometry, most especially in the rounding of the corners, have a significant effect on the response of the foam, captured in both experiment and simulation. On the other hand, foam properties such as bubble size have little impact on the rheological behavior of the foam in the range considered here. © *2012 The Society of Rheology*. [http://dx.doi.org/10.1122/1.3687301]

I. INTRODUCTION

Aqueous foams are familiar materials due, in part, to their use in domestic washing applications as well as a host of other domestic and industrial processes [Cantat *et al*. (2010); Weaire and Hutzler (1999)]. During washing, the surfactant that acts as a detergent also stabilizes the foam, and the foam that often results from agitation of the wash liquor is perceived as a measure of the efficacy of the wash. It is therefore of interest to determine the extent to which a given surfactant mixture creates a stable foam which can survive non-negligible perturbations.

Constriction, or contraction/expansion, flow has proved very useful in the past as a means of testing the behavior of polymers and other complex fluids when exposed to both shear and extensional strain [Binding and Walters (1988)]. A number of previous experimental studies of foam flow through constrictions have been carried out, and these are reviewed by Jones *et al*. (2011). We describe here a benchmark constriction flow of a stable foam to give a baseline rheological response unaffected by bursting. We employ a two-dimensional (2D) or Hele-Shaw geometry (a monolayer of bubbles) since this allows us to ascertain the position and shape of each bubble at all times without requiring expensive and slow 3D imaging.

[a]Present address: Institut de Physique de Rennes, Université Rennes 1, 35042 Rennes, France.
[b]Author to whom correspondence should be addressed; electronic mail: sxc@aber.ac.uk

Given the ranges of material parameters of foams found in applications and the numerous geometries within which foams are made to flow, our goal is also to develop a simulation tool that can accurately predict foam response in a broad range of situations. This will lead to the ability to determine optimal flow conditions and foam parameters without recourse to costly and time-consuming experiments. The constriction geometry is ideal for the purpose of validating such a tool, since both shear and extensional components of the stress are nontrivial and wall-slip may be significant. Here, we describe the results of 2D simulations of a dry foam using Surface Evolver [Brakke (1992)] with the same geometry as the experiment. The simulations are quasistatic, the most appropriate choice for slow flows of dry foams. We are, therefore, in a position to compare experiments and simulations in detail and draw conclusions about the efficacy of these simulations in predicting the flow.

The plan of this paper is as follows. Our methods are described in Sec. II. The results of the reference experiment are compared with a quasistatic simulation in Sec. III. Changes to the bubble size, the rounding of the constriction corners, the flow velocity, and the depth of the channel are then made, and the effects of these changes, both in experiment and in simulation, are discussed in Sec. IV. Finally, we draw some conclusions in Sec. V and speculate on the extension of this work to less stable foams.

II. METHODS

A. Experimental set-up

Experiments were carried out using a Hele-Shaw cell with side-wall profiles cut from Polytetrafluoroethylene (PTFE) sheet. These constriction profiles were sandwiched between two parallel horizontal glass plates to form a channel of length $L = 70$ cm and width $W = 12$ cm (Fig. 1). A constriction ratio of 4:1 was obtained by setting $c_W = 4.5$ cm, and the length of the constricted region was $c_L = 3$ cm. The profiles were either cut with square corners ($\epsilon \approx 0$) or with rounded corners ($\epsilon = 0.5 \pm 0.1$ cm), where ϵ is the radius of curvature of the corner. Various thicknesses of PTFE sheet are available, and tests were carried out with a channel depth of either 0.15 cm or 0.3 cm. We observe almost full slip at the wall.

The foaming solution was 5% fairy liquid in deionised water. Foam was created by blowing compressed air through a nozzle in the base of the bubble chamber (Fig. 2), and the overpressure generated in the bubble chamber created the driving force for the foam flow through the Hele-Shaw cell. The volumetric flow rate can be varied: we used $Q = 0.023$ litres per minute (lpm) for the channel of depth 0.15 cm, and for the deeper channel (0.3 cm) we used either twice this value ($Q = 0.046$ lpm, giving the same free-stream velocity) or a value of $Q = 0.104$ lpm to test the effects of the free-stream velocity. The bubble size of the foam can also be varied in the range $0.09 \pm 0.02\,\mathrm{cm}^2$ to $0.19 \pm 0.04\,\mathrm{cm}^2$.

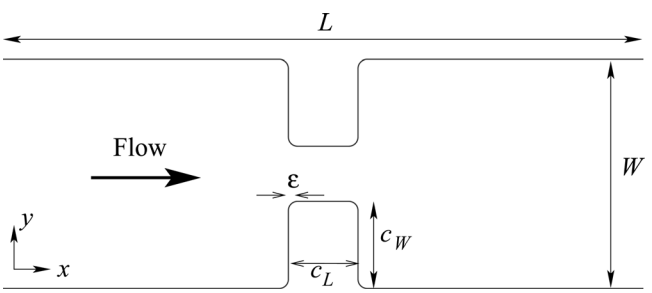

FIG. 1. Schematic representation of the constriction.

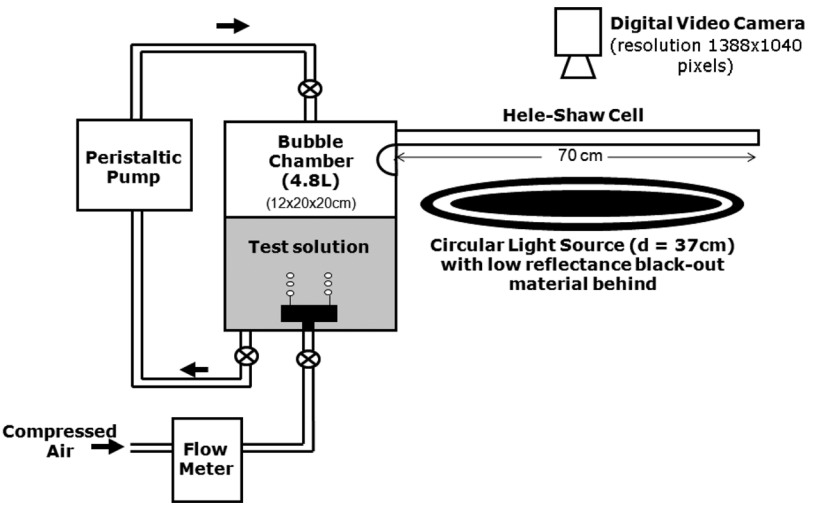

FIG. 2. Schematic representation of the experiment.

The Hele-Shaw cell is backlit by a circular (diameter 37 cm) fluorescent tube, with a central dark field so that soap films appear white with good contrast. The motion of the foam was recorded using a high resolution (1388×1040 pixels) digital video camera running at 20 fps; this camera allows us to image a larger field of view than Jones *et al.* (2011), giving better information about the deviation from a plug flow upstream and downstream, and to plot the results on a finer grid, enabling more detail of the flow to be seen. A typical image of the foam flow is given in Fig. 3.

B. Image analysis

Image analysis was carried out using the IMAGEJ software package with added morphology, particle tracking, Delauney triangulation, and edge information plugins [Rasband (1997–2007)].

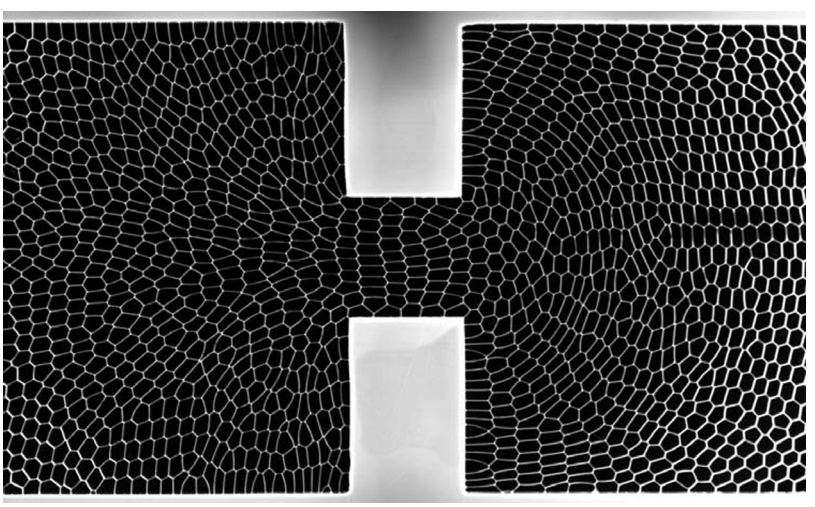

FIG. 3. Photograph of the experiment, with soap films shown in white. The square ($\epsilon \approx 0$) constriction profile is shown with the reference foam (average bubble area $= 0.093 \pm 0.02\,\mathrm{cm}^2$).

The center of a bubble was defined as the average of the x and y coordinates for all the pixels in that bubble. The morphology plugin was used to identify the locations of all the bubble centers for each image, and the particle tracking plugin was then used to follow the trajectories of individual bubble centers. The average bubble velocity distribution was calculated, using a C program, by defining $\underline{V} = (V_x, V_y)$ to be the displacement of bubble centers between frames, averaged over a subsection of the whole image. These subsections were defined by a 20×15 grid for plotting line profiles, and a 60×45 grid for plotting fields. All velocities are scaled by the free-stream velocity, V_0, measured as the velocity upstream of the constriction in the center of the channel.

The velocity profile allows the local deformation rate to be calculated using

$$\underline{\underline{D}} = \begin{bmatrix} \dfrac{\partial V_x}{\partial x} & \dfrac{1}{2}\left(\dfrac{\partial V_x}{\partial y} + \dfrac{\partial V_y}{\partial x}\right) \\ \dfrac{1}{2}\left(\dfrac{\partial V_x}{\partial y} + \dfrac{\partial V_y}{\partial x}\right) & \dfrac{\partial V_y}{\partial y} \end{bmatrix}. \tag{1}$$

The tensor is diagonalized and the eigenvalues and eigenvectors calculated. These are then plotted as a way of visualizing the local magnitude and direction of the maximum rates of elongation and compression throughout the constriction [Dollet (2010)].

A Delauney triangulation gives the lines joining adjacent bubble centers, which allows us to calculate the texture tensor $\underline{\underline{M}}$, an indication of the local strain [Graner *et al*. (2008)]. Note that this Delauney method is not quite equivalent to an average over the links joining touching bubbles, as recommended [Graner *et al*. (2008)] and as used in the simulations, but away from the boundary we are unable to distinguish the results. The full texture tensor can be represented with ellipses [Graner *et al*. (2008)], over the same grid as the velocity, and its normalized extensional component [Jones *et al*. (2011)],

$$M_n = \frac{M_{xx} - M_{yy}}{M_{xx} + M_{yy}}, \tag{2}$$

used to plot line profiles.

The original foam image was also skeletonized and the edge information plugin used to extract information on the length, orientation, and position of each bubble film, assumed straight. The components of the elastic stress corresponding to shear (σ_{xy}) and extension ($\sigma_{xx} - \sigma_{yy}$) were then calculated by integrating the tension forces along each edge [Batchelor (1967); Cox and Whittick (2006)]. The total foam area and the individual bubble areas are not consistent between experiment and simulation, however, so to facilitate comparison, the shear and extensional stresses are rescaled by the total elastic stress [Dollet (2010)]

$$\frac{(\sigma_{xy})}{(\sigma_{xx} + \sigma_{yy})} \quad \text{and} \quad \frac{(\sigma_{xx} - \sigma_{yy})}{(\sigma_{xx} + \sigma_{yy})}, \tag{3}$$

respectively.

The experimental data were averaged over 4000 frames. For all the plots, a region of the test section of length 20 cm and width 12 cm is considered, centered on the middle of the constriction, a region roughly equivalent to that of the simulation.

C. Simulations

We use the Surface Evolver [Brakke (1992)] to perform a quasistatic 2D simulation of disordered foam flowing through the constricted channel. The channel has unit length $L = 1$ and width $W = 0.5$, and the constricted region has $c_L = 0.15$ and $c_W = 0.19$, see Fig. 4. There are free-slip boundary conditions on the channel walls, and bubbles going out at the right re-enter on the left (periodic boundary condition, PBC).

The foam is created from a Voronoi diagram based on randomly distributed seedpoints, [Brakke (1986)], and target bubble areas specified within Surface Evolver. Since the pressure difference across each film is constant, the Young-Laplace law implies that each film can be represented as a circular arc. We chose a cut-off length for the neighbor-switching topological changes that is appropriate to simulate the effect of a liquid fraction of 10^{-5} [Raufaste *et al.* (2007)]. Foams of up to $N = 725$ bubbles were simulated for 1000 iterations, which take up to 2 weeks on a desktop PC. The bubble size is, therefore, equal to $(LW - 2c_L c_W)/N$, with a slight dispersity (normalized standard deviation of 18%) introduced to prevent crystallization of the foam, fixed for the duration of the simulation.

Each iteration consists of choosing a line of films that span the channel upstream of the constriction and moving them downstream a small distance $\mathrm{d}x$ [Raufaste *et al.* (2007)], before finding a minimum of surface energy (total perimeter). In this way, the foam proceeds through a sequence of equilibrium states, appropriate to a situation where the foam moves very slowly and viscous effects may be neglected.

We calculate the center of each bubble as an average of its vertex positions, so that in this way the displacement between iterations (velocity) can be found. The instantaneous texture tensor is found by averaging the components of the line joining the bubble centers adjacent to each film. Stress is calculated by integrating the surface tension along each arc and summing. We assume that the flow is steady and average the data over 1000 iterations on a 60×30 grid.

III. RESULTS: REFERENCE CASE

For the reference experiment, a channel depth of 0.15 cm and square corners ($\epsilon = 0$ cm) were chosen. The foam had an average bubble size of $0.093 \pm 0.020\,\mathrm{cm}^2$, a liquid fraction of $\phi_l \approx 0.003$, and a free-stream velocity of $V_0 = 0.13$ cm/s. The reference simulation had $N = 725$ bubbles and $\epsilon = 0.01$ (it is not possible to simulate perfectly square corners because of the singularity in the gradient). At each iteration, the foam is moved downstream a distance $\mathrm{d}x = 0.001$.

We compare the fields of velocity, texture, stress, and deformation rate to ascertain the level of qualitative agreement between experiment and simulation, before making a

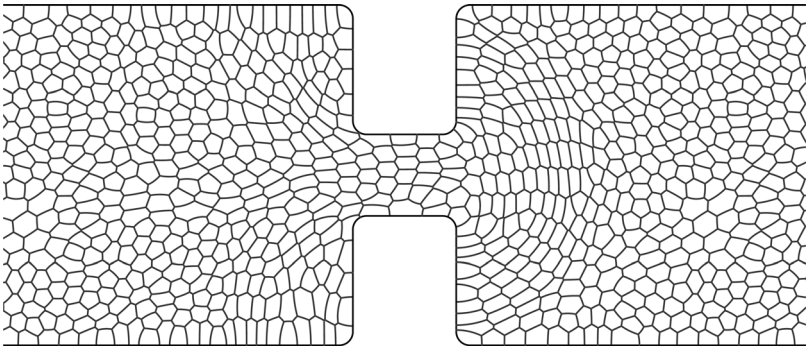

FIG. 4. Image from simulation. In this case, $N = 704$, $L = 1$, $W = 0.5$, $c_L = 0.15$, $c_W = 0.19$, $\epsilon = 0.02$.

quantitative comparison of these measures along lines drawn along (centerline) and across (transverse) the geometry.

A. Velocity

The magnitude of the velocity, V_{mag}, is shown in Fig. 5(a): both simulation and experiment show the same features, in particular, the fan-shaped profile upstream of the constriction and the semicircular profile downstream of the constriction, with a good agreement in terms of contour locations. For the magnitude of the transverse component of velocity V_y, shown in Fig. 5(b), both simulation and experiment show distinct lobes

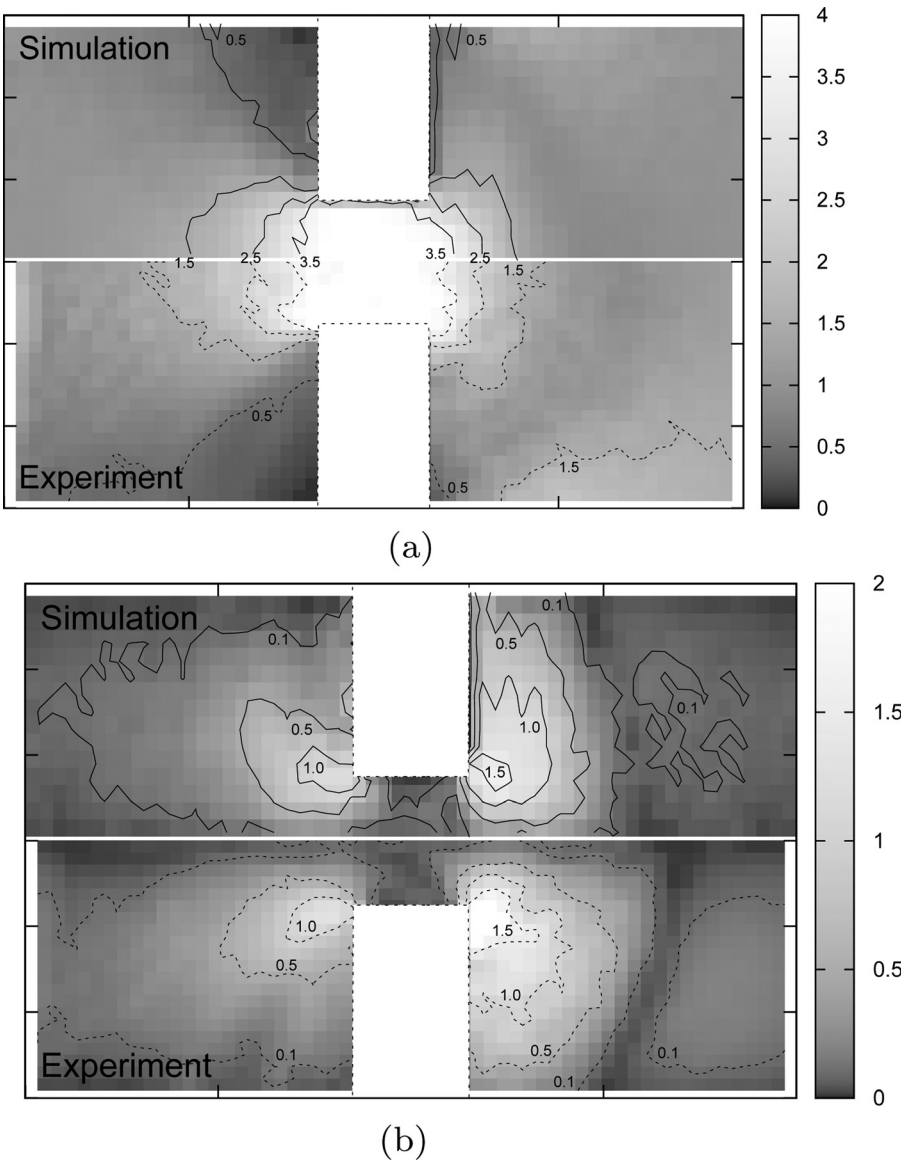

FIG. 5. Fields of: (a) velocity magnitude V_{mag} normalized by V_0, with contours at 0.5, 1.5, 2.5, and 3.5; and (b) magnitude of the vertical component of velocity, V_y normalized by V_0, with contours at 0.1, 0.5, 1.0, and 1.5. In each plot, the upper half shows the simulation result, and the lower half shows the experimental result.

downstream and distinct tails upstream of the constriction. However, in both cases, the simulation shows a much more localized effect of the constriction, with the lobes in V_y downstream of the constriction extending a shorter distance than in the experiment. The simulation also suggests higher velocity in the upstream corners [Fig. 5(a)], possibly because of the small amount of rounding ($\epsilon = 0.01$) at these corners; in the experiment, the extent of the lower velocity region in the upstream corners is much larger (contour of $V_{\text{mag}} = 0.5$), and it is not uncommon for bubbles to become stuck in these corners, causing small stagnation zones. We observed no evidence of recirculation zones either upstream or downstream.

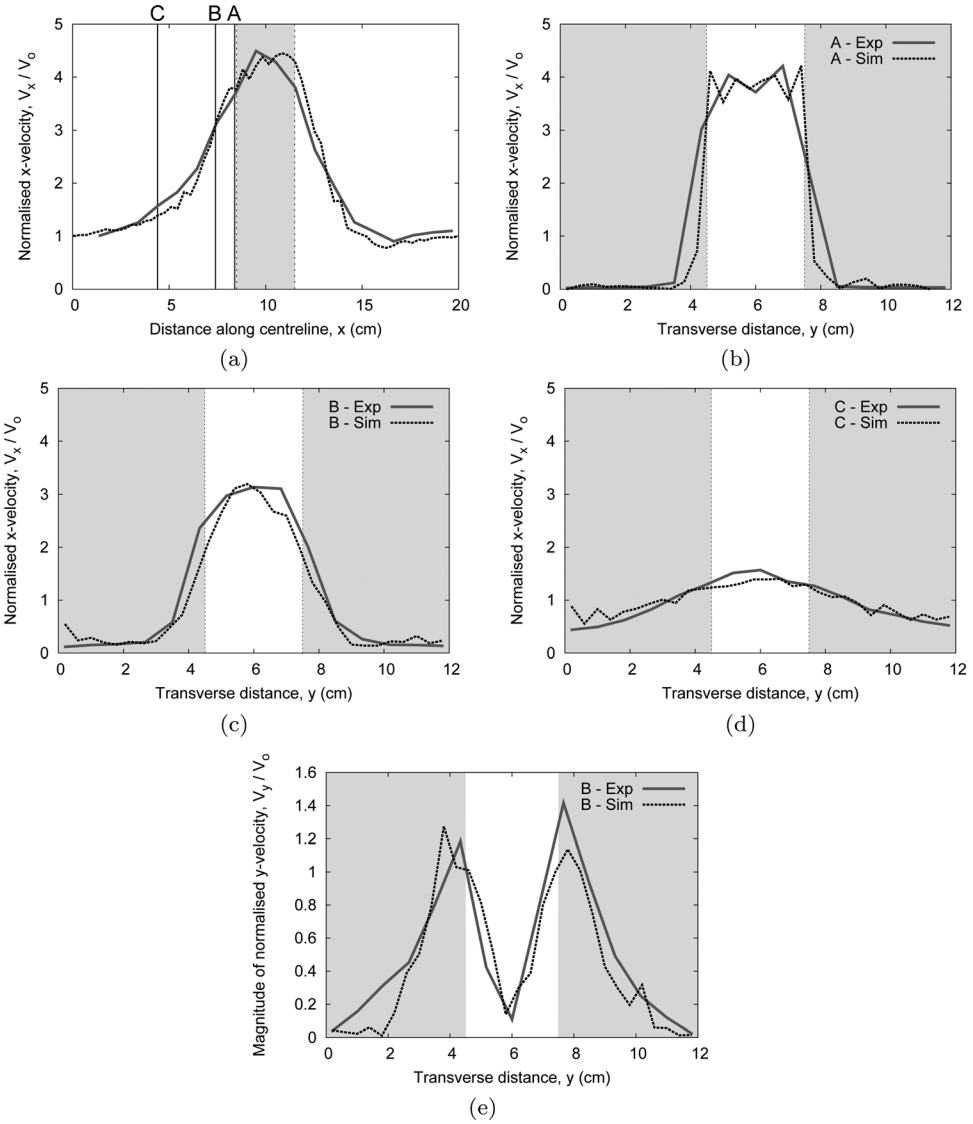

FIG. 6. Velocity profiles from the reference experiment are shown with solid gray lines and from the reference simulation with dashed black lines. In all cases, the location of the constriction is indicated by the shaded areas. The x-component of velocity V_x, on (a) the centerline of the constriction; (b) transverse slice **A** just upstream of the constriction entrance; (c) transverse slice **B**, one grid box upstream of **A**; (d) transverse slice **C**, four grid boxes upstream of **A**. (e) The y-component of velocity V_y on transverse slice **B**.

More accurate indicators of the agreement between experiment and simulation are the centerline and transverse profiles of velocity, as they give a quantitative measure of the foam's behavior (Fig. 6). The three transverse profiles for V_x are taken along three columns of grid boxes directly upstream of the constriction. The center points of these grid boxes are indicated in Fig. 6(a) and are equivalent to distances of 0, 1, and 4 cm upstream of the constriction (approximately 0, 3, and 12 bubble diameters, respectively).

Both the longitudinal and transverse plots show some small discrepancies between the experiment and simulation: along the centerline, the velocity begins to rise further upstream of the constriction in experiment, a feature also observed on the transversal C [Fig. 6(d)]; and the return to the free-stream velocity also occurs further downstream than in the simulation. Both the experiment and simulation show an asymmetry of V_y about the centerline [Fig. 6(e)] but this variation is within the error bars of the experimental results (the error in V_x/V_0 is approximately ± 0.22).

B. Texture

The texture tensor $\underline{\underline{M}}$ is shown as ellipses in Fig. 7(a), demonstrating the magnitude and direction of the local strain acting on the foam. Upstream of the constriction, all these ellipses are angled toward the entrance to the constriction, before aligning themselves along the direction of flow within the constriction. At the exit from the constriction, the local strain undergoes an abrupt 90° change in direction, with the ellipses now forming a broad semicircular pattern around the exit.

To obtain a quantitative comparison between experiment and simulation we plot the centerline profile of the normalized extensional component of $\underline{\underline{M}}$, Eq. (2), which measures the stretching of the bubbles, in Fig. 7(b). In the simulation, M_n rises smoothly from its free-stream value to a broad peak, with the maximum at the entrance to the constriction. The value of M_n starts decreasing rapidly just upstream of the constriction exit and drops to a minimum, of the same magnitude as the initial peak, before finally returning to its initial value at the exit of the test section.

In comparison, the experiment shows a much noisier profile; the maximum value of M_n occurs further downstream, within the constriction itself; the minimum in M_n that occurs after the constriction also occurs further downstream and is much broader than in the simulation. Both the initial peak in M_n and the minimum downstream show a smaller magnitude in experiment than the simulation predicts. However, the steep drop in M_n immediately downstream of the constriction, where the bubble shape and orientation are changing the fastest, shows an excellent agreement between experiment and simulation.

It should be noted that within the experimental test section, the texture does not return to zero upstream or downstream, indicating that the constriction is far-reaching in its effect on bubble deformation. In the simulation, on the other hand, the PBCs force M_n to return to zero. This suggests that the use of PBCs results in an underestimate of the deformation of the foam [Jones *et al*. (2011)], but simulations with longer channels (data not shown) indicate that the texture returns to zero at the same distance downstream, emphasizing that this prediction is robust. We speculate that this more rapid return of the bubble shape to an isotropic state is due to the lack of viscous effects in the simulation, removing a mechanism by which the deformation could be advected downstream.

C. Stress

The fields of the rescaled shear and extensional components of the elastic stress are shown in Fig. 8. There is a good agreement between experiment and simulation, for example in the locations of the maxima and minima. However, the simulated fields are

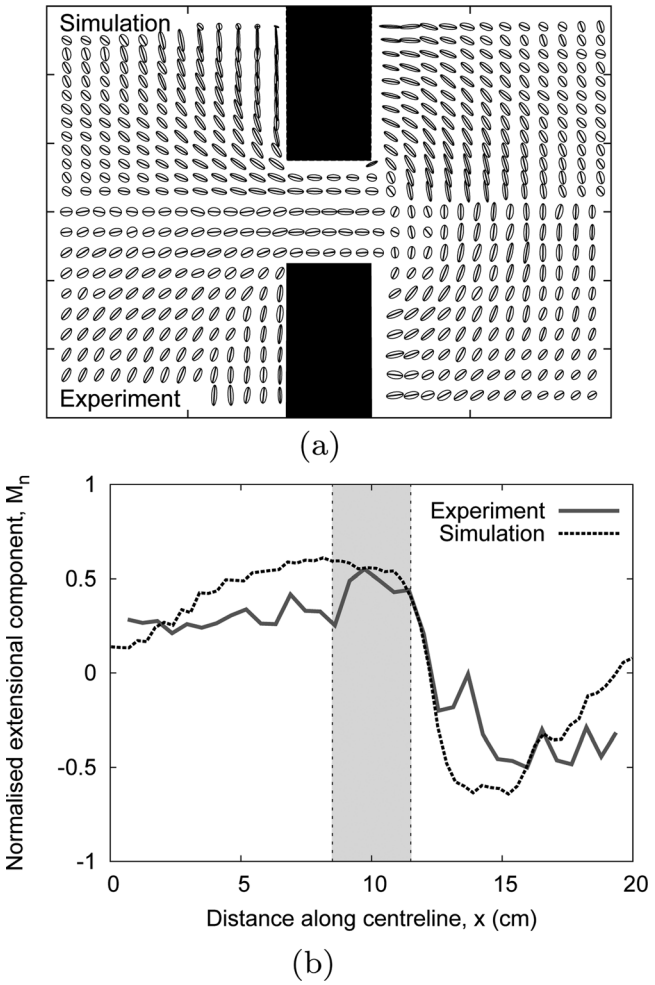

FIG. 7. (a) Texture field for experiment shown as an ellipse plot, with the simulation result in the top half and the experimental result in the bottom half. (b) Profile of normalized texture M_n along the centerline of the constriction for experiment and simulation. The experimental result is shown with the solid gray line and the quasi-static result with the dashed black line.

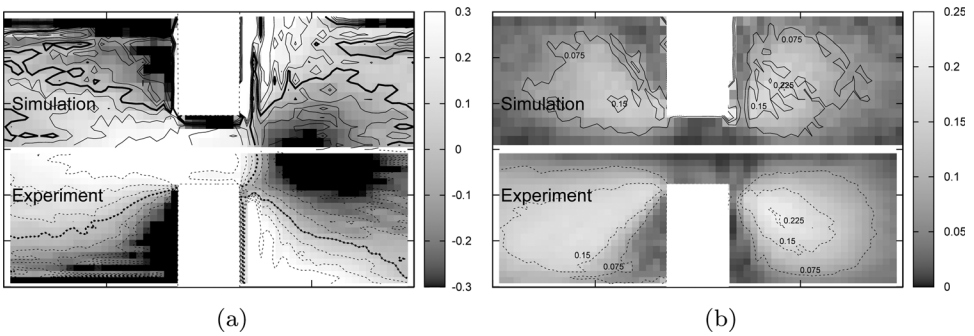

FIG. 8. (a) Rescaled extensional stress $(\sigma_{xx} - \sigma_{yy}/\sigma_{xx} + \sigma_{yy})$, with contours at intervals of 0.1 from − 0.3 to 0.4. The contour at 0 is shown in bold. (b) Magnitude of the rescaled shear stress $(\sigma_{xy}/\sigma_{xx} + \sigma_{yy})$, with contours at 0.075, 0.15, and 0.225. The top half of each plot shows the simulation result, and the lower half of each plot shows the experimental result.

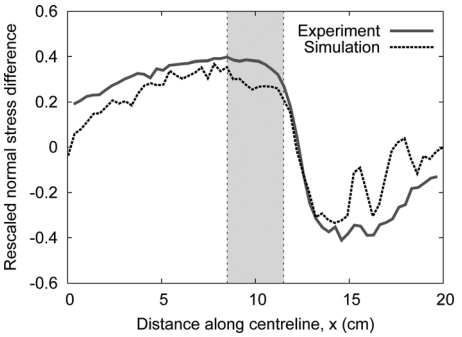

FIG. 9. Normal stress difference (extensional stress) rescaled by the total elastic stress, $(\sigma_{xx} - \sigma_{yy})/(\sigma_{xx} + \sigma_{yy})$.

slightly noisier than the experimental fields, presumably due to the smaller number of bubbles being considered.

The rescaled extensional stress along the centerline is shown in Fig. 9: in the experiment, it rises further upstream and returns to the free-stream value further downstream, after the constriction, just as for the texture; again, we speculate that it is the neglect of viscous effects in the simulation that causes the stresses to relax more quickly as the foam moves away from the constriction region.

D. Deformation rate

The local deformation rate $\underline{\underline{D}}$ is shown in Fig. 10. To facilitate comparison, $\underline{\underline{D}}$ is rendered dimensionless by rescaling velocities by the free-stream velocity, V_0, and distances by the width of the channel, W. There are clear regions of high deformation rate at the entrance and exit of the constriction, although these regions are, as for the velocity, more localized in simulation than in experiment.

There is also an agreement between experiment and simulation with respect to two other features in the deformation rate. In both cases, there is a distinct minimum in the magnitude of the deformation rate within the constriction. There is also a flip in the direction of the eigenvalues across the constriction, with the initially streamwise elongation

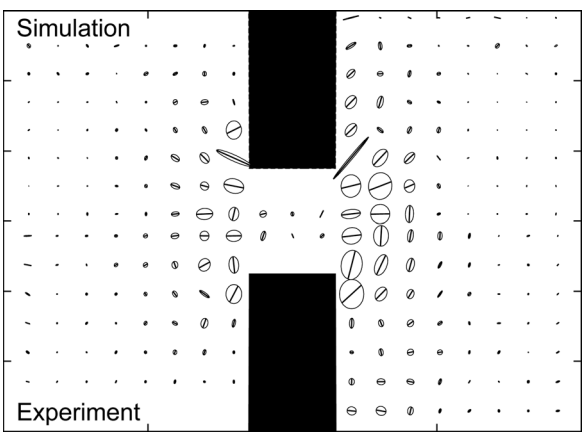

FIG. 10. Deformation rate measured in the simulation (top half) and the experiment (lower half). The black lines represent the positive eigenvalue of $\underline{\underline{D}}$ corresponding to elongation, and the gray lines the negative eigenvalue corresponding to compression.

orienting itself transverse to the flow at the exit of the constriction, a change similar to that seen in the texture, Fig. 7(a).

IV. RESULTS: PARAMETER VARIATION

The simulation performs remarkably well at predicting the dynamics of the experiment. Close to the constriction, the agreement between velocity, deformation rate, strain and stress is good. Texture and stress tail off more slowly than velocity, so we turn to the velocity as a means to determine whether the agreement holds when we change the parameters of the experiment from the reference case. We will use the x-component of the velocity on the centerline and on transversal A and the y-component of the velocity on transversal B to compare the effects of changing corner curvature, channel depth, free-stream velocity and bubble size. The transverse plots are included as they give the best picture of the foam behavior in the corners upstream of the constriction.

A. Corner rounding

Rounding the corners of the constriction, changing the value of ϵ from close to 0 to 0.5 ± 0.1 cm in experiment and from 0.01 to 0.02 and 0.069 in simulation, has a significant effect on the flow, with the peak in the centerline velocity profile becoming smoother, narrower, and more symmetrical [Fig. 11(a)]. This is seen in both the experimental results and the simulation.

The transverse velocity profiles [Fig. 11(b)] in the simulation show that the peak in the velocity again becomes smoother, and the small peaks at the edges of the constriction disappear. In the experiment, there is a notable increase in the velocity at the side-walls, near the upstream corners of the constriction, compared to the square case. This reflects the qualitative observation (Sec. III A) that the foam was seen to move round the upstream corner much more freely with a rounded profile. This easing of the flow is reflected in a drop in the extensional stress (data not shown) in both experiment and simulation. The profiles of V_y [Fig. 11(c)] reinforce this message: the simulation at large ϵ shows enhanced flow velocities in the upstream corners.

B. Channel depth

By changing the plate separation in the experiment, we explore the effect of friction between the soap films and the bounding glass plates. Increasing the plate separation should reduce the effect of the friction and move closer to the predictions of the simulation.

Thus, we compare the reference case results for experiment and simulation with an experiment at twice the thickness ($d = 0.3$ cm). Perhaps surprisingly, the prediction gets slightly worse [Figs. 11(d)–11(f)], suggesting that the 2D approximation no longer holds and that the films start to curve across the gap [Grassia *et al*. (2008)].

C. Free-stream velocity

Since the simulations are quasistatic it is not possible to change the flow-rate. In the experiment, however, we more than doubled the flow-rate, increasing the free-stream velocity by a factor of about 2.2, in order to determine the extent to which the experiments are in the quasistatic regime. The results, shown in Figs. 11(g)–11(i), indicate that the effect on the normalized velocity field is greater upstream than downstream of the constriction, with the simulations underestimating the x-component of the velocity there. The graph of V_y [Fig. 11(i)] suggests that the streamlines curve toward the constriction further downstream than at low velocity.

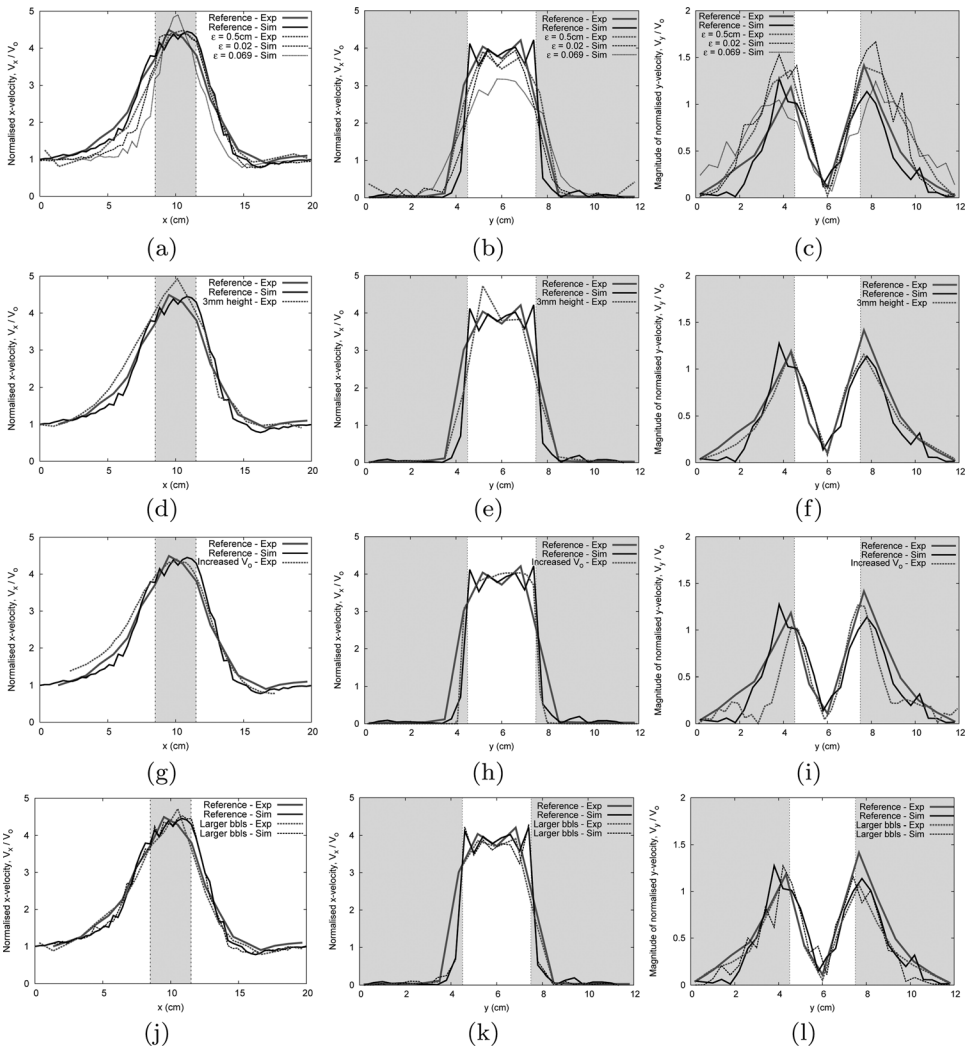

FIG. 11. Variation of parameters. The results for all variations are compared with the reference experiment (solid gray line) and simulation (solid black line). First column: x-component of the velocity along the centerline. Second column: x-component of the velocity on transversal **A**. Third column: magnitude of y-component of the velocity on transversal **B**. First row: increased rounding of the corners. Second row: increased experiment thickness. Third row: increased free-stream velocity. Fourth row: increased bubble size.

D. Bubble size

Changing the bubble size relative to the geometry of the constriction allows us to explore how far from the continuum limit we are, especially since large N is not currently achievable with our simulations. We increase the bubble size to see how the experimental result changes and whether the simulations are still accurate in predicting the flow.

The bubble size was roughly doubled in experiment, compared to the reference case, to $0.193 \pm 0.039\,\mathrm{cm}^2$, and increased by roughly 35% (N reduced from 725 to 539) in the simulation. This makes little difference to the simulation result [Figs. 11(j)–11(l)]: the velocity plots are slightly coarser, and the reduction in the number of bubbles also seems to affect the smoothness of the stress (data not shown). The same invariance is seen in the experimental result, suggesting that although many bubbles will give better statistics and

smoother profiles, the essence of the flow is captured with even a coarse approximation. This is useful in terms of simulation processing times as there appears to be no need to simulate very larger numbers of bubbles to obtain useful results.

V. DISCUSSION

The reference case provides a useful comparison between the experiment and a quasistatic simulation. In general, the simulation makes excellent predictions, even if the experiment might not truly be in the quasistatic regime.

There is a very good agreement in terms of velocity fields and velocity profiles, with any discrepancies falling within the range of the error bars of the experiment. This agreement extends to the calculation of deformation rate, with, again, a very good agreement between experiment and simulation, with any variations falling within the uncertainty in the results.

Fields of both texture (strain) and elastic stress are also in accord, although here a reduction in the range of the effect of the constriction is apparent in the simulation, which we attribute to the quasistatic approximation. This is something that could and should be tested in future work.

Of the quantities considered, the ones most suited to comparing experiment and simulation are the centerline velocity profile and a transverse velocity profile close to the constriction.

A. Parameter variation

Rounding the corners of the constriction, i.e., increasing ϵ, has a significant effect on the foam flow behavior, giving smoother velocity profiles, lower stresses and more flow round the upstream corners.

Increasing the channel depth or the free-stream velocity both reduce the agreement between simulation and experiment; the best agreement occurs when the experiment is closest to a 2D system, despite the probable increase in the effective friction, and when the velocity is lowest, which reduces the effect of friction. Larger plate separation (channel depth) does not give greater flow in the upstream corners, as might be expected, suggesting that on the occasions when bubbles get stuck in the upstream corners this is not a result of friction at the bounding glass plates.

Increasing the bubble size by up to 100% has little effect on the experimental or simulation results. Although reducing the bubble size means that the continuum limit will be more closely approximated, giving better statistics and smoother profiles, the basic behavior of the flow is captured with a coarse approximation.

In summary, in terms of altering the behavior of a flowing foam, changing the foam's material properties (bubble size) has little effect in comparison to changes in flow geometry and speed. The most significant factor in changing the flow behavior captured by both simulation and experiment is the value of ϵ, i.e., how rounded the corners of the constriction are, with only small changes in ϵ producing major changes to the flow behavior. Experiments also show that as the foam moves more quickly the quasistatic simulations become less useful.

B. Foam stability

We deliberately chose a surfactant that gives stable foams at liquid fractions in the range 0.001–0.01. When older, and therefore drier, foams or chemically more fragile mixtures are used, film breakage has been observed in regions where films are rapidly stretched. This can occur in several ways: just after T1 topological changes, in the regions of high

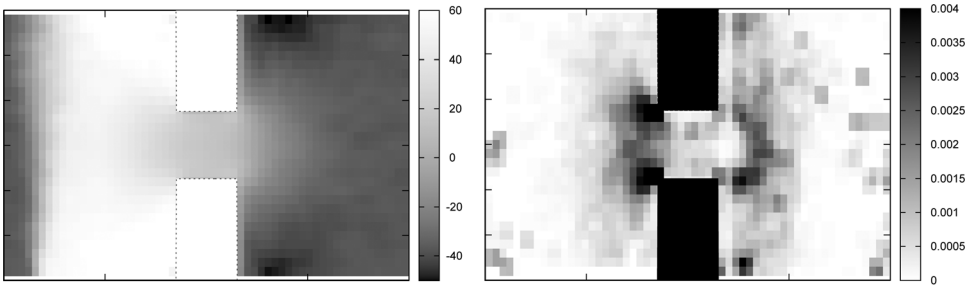

FIG. 12. (a) Bubble pressures are given by Surface Evolver as the Lagrange multiplier of the area constraint on each bubble, allowing the calculation of the time-averaged pressure field in the reference case. (b) The position of each neighbor-switching change in topology (T1) is recorded unambiguously in the simulations, allowing this "plasticity" map of T1 frequency to be generated.

deformation rate at the entrance and exit to the constriction, and when larger bubbles/voids move at a high relative velocity through the foam [Cantat and Delannay (2003)].

Our ongoing work now seeks to measure the positions of T1 topological changes and calculate bubble pressures in the experiments, in order to further test the predictions of the quasistatic model shown in Fig. 12; to understand the influence of foam composition; and to predict where in the foam the films may first fail, leading to the partial or global destruction of the foam.

ACKNOWLEDGMENTS

The authors are grateful to B. Dollet and P. Grassia for useful discussions, to D. Francis, J. Parry, and A. Rawlins for technical and computing support, to K. Brakke for assistance with Surface Evolver, and to EPSRC (EP/D071127/1) and the P&G/EPSRC strategic partnership (EP/F000049/1) for financial support.

References

Batchelor, G. K., *An Introduction to Fluid Dynamics* (Cambridge University Press, Cambridge, 1967).

Binding, D. M., and K. Walters, "On the use of flow through a contraction in estimating the extensional viscosity of mobile polymer solutions," J. Non-Newtonian Fluid Mech. **30**, 233–250 (1988).

Brakke, K., "The Surface Evolver," Exp. Math. **1**, 141–165 (1992).

Cantat, I., and R. Delannay, "Dynamical transition induced by large bubbles in two-dimensional foam flows," Phys. Rev. E **67**, 031501 (2003).

Cantat, I., S. Cohen-Addad, F. Elias, F. Graner, R. Höhler, O. Pitois, F. Rouyer, and A. Saint-Jalmes, *Les Mousses—Structure et Dynamique* (Belin, Paris, 2010).

Cox, S. J., and E. L. Whittick, "Shear modulus of two-dimensional foams: The effect of area dispersity and disorder," Eur. Phys. J. E **21**, 49–56 (2006).

Dollet, B., "Local description of the two-dimensional flow of foam through a contraction," J. Rheol. **54**, 741–760 (2010).

Graner, F., B. Dollet, C. Raufaste, and P. Marmottant, "Discrete rearranging disordered patterns, part I: Robust statistical tools in two or three dimensions," Eur. Phys. J. E **25**, 349–369 (2008).

Grassia, P., G. Montes-Atenas, L. Lue, and T. E. Green, "A foam film propagating in a confined geometry: Analysis via the viscous froth model," Eur. Phys. J. E **25**, 39–49 (2008).

Jones, S. A., B. Dollet, N. Slosse, Y. Jiang, S. J. Cox, and F. Graner, "Two-dimensional constriction flows of foams," Colloids Surf., A **382**, 18–23 (2011).

Rasband, W. S., *ImageJ* (U.S. National Institutes of Health, Bethesda, Maryland, 1997–2007), http://rsb.info.nih.gov/ij/

Raufaste, C., B. Dollet, S. Cox, Y. Jiang, and F. Graner, "Yield drag in a two-dimensional foam flow around a circular obstacle: Effect of liquid fraction," Eur. Phys. J. E **23**, 217–228 (2007).

Weaire, D., and S. Hutzler, *The Physics of Foams* (Clarendon, Oxford, 1999).